

THE *BEPPOSAX* HIGH ENERGY LARGE AREA SURVEY – V. THE NATURE OF THE HARD X-RAY SOURCE POPULATIONS AND ITS EVOLUTION

F. LA FRANCA,¹ F. FIORE,² C. VIGNALI,³ A. ANTONELLI,² A. COMASTRI,⁴ P. GIOMMI,⁵ G. MATT,¹
S. MOLENDI,⁶ G. C. PEROLA,¹ F. POMPILIO⁷

Received 2001 October 31; Accepted 2002 January 10; To appear on *ApJ*, volume 570, May 1, 2002

ABSTRACT

We present optical spectroscopic identifications of hard X-ray (5-10 keV) selected sources belonging to the HELLAS sample obtained with *BeppoSAX* down to a 5-10 keV flux limit of $f_{5-10\text{keV}} \sim 3 \times 10^{-14}$ erg cm⁻² s⁻¹. The sample consists of 118 sources. 25 sources have been identified through correlations with catalogues of known sources. 49 have been searched for spectroscopic identification at the telescope. 13 fields resulted empty down to R=21. 37 sources have been identified with type 1 AGN and 9 with type 2 AGN. The remaining are: 5 narrow emission line galaxies, 6 Clusters, 2 BL Lac, 1 Radio Galaxy and 1 Star. Combining these objects with other hard X-ray selected AGNs from *ASCA* and *HEAO1*, we find that the local luminosity function of type 1 AGN in the 2-10 keV band is fairly well represented by a double-power-law-function. There is evidence for significant cosmological evolution according to a pure luminosity evolution (PLE) model $L_X(z) \propto (1+z)^k$, with $k=2.12$ and $k=2.22$ ($\sigma_k \simeq 0.14$) in a $(\Omega_m, \Omega_\lambda)=(1.0, 0.0)$ and in a $(\Omega_m, \Omega_\lambda)=(0.3, 0.7)$ cosmology, respectively. The data show an excess of faint high redshift type 1 AGN which is well modeled by a luminosity dependent density evolution (LDDE), similarly to what observed in the soft X-rays. However, in both cosmologies, the statistic is not significant enough to distinguish between the PLE and LDDE models. The fitted models imply a contribution of AGN1 to the 2-10 keV X-ray background from 35% up to 60%.

Subject headings: cosmology: observations — galaxies: distances and redshift — galaxies: evolution — galaxies: active — quasars: general

1. INTRODUCTION

AGN have first been discovered in the radio and soon after searched in the optical band. Consequently, they have been classified using their optical characteristics and mainly divided into two categories: type 1 (AGN1) and 2 (AGN2) according to the presence or not of broad emission lines in their optical spectra (we will keep this definition of AGN1 throughout this paper).

Before the advent of the last generation of hard X-ray telescopes, AGN samples were predominantly based on AGN1 selected either in the optical or, later on, in the soft X-rays by *Einstein* and *ROSAT*. In these bands the evolution of AGN1 has been well measured (see e.g. Della Ceca et al. 1992; Boyle et al. 2000; Miyaji, Hasinger, & Schmidt 2000). On the contrary the production of samples of AGN2 has been difficult at any wavelength and limited to few local surveys.

The general picture was in favor of a model in which AGN1 objects were associated to AGN with low absorption in the hard X-rays while AGN2 to obscured sources with large column densities and spectra strongly depressed in the soft X-rays, as expected in the unification models (e.g. Antonucci 1993).

In the last decade the advent of the *ASCA* and *BeppoSAX* satellites has allowed for the first time the detec-

tion and identification of AGN as the main counterparts of hard (2-10 keV) X-ray sources down to fluxes $\sim 5 \times 10^{-14}$ erg cm⁻² s⁻¹, more than 2 orders of magnitude fainter than *HEAO1* (Wood et al. 1984). These identifications accounted for about 30% of the 2-10 keV hard X-ray background (Ueda et al. 1998; Fiore et al. 1999). Recently the new generation of X-ray satellites such as *Chandra* and *XMM-Newton*, have reached fluxes 100 times fainter, identifying hundreds of sources and almost resolving the hard (2-10 keV) X-ray background (e.g. Mushotzky et al. 2000; Fiore et al. 2000; Giacconi et al. 2001; Hornschemeier et al. 2001; Hasinger et al. 2001; Tozzi et al. 2001; Baldi et al. 2001).

Thanks to their excellent angular resolution ($\sim 1-5''$), the first spectroscopic identifications projects have been able to observe faint (I \sim 23) optical counterparts. At variance with the classical type-1/type-2 model in the optical, a significant number of the counterparts ($\sim 30\%$) resulted to be apparently optical normal galaxies, with X-ray luminosities $L_X \simeq 10^{42} - 10^{44}$ erg s⁻¹ typical of AGN activity, and moreover part of the optical type 1 AGNs resulted to be absorbed in the hard X-rays (see e.g. Fiore et al. 2000; Barger et al. 2001; Tozzi et al. 2001; Hornschemeier et al. 2001; Comastri et al. 2002).

These observations have complicated the picture of the

¹Dipartimento di Fisica, Università degli Studi Roma Tre, Via della Vasca Navale 84, I-00146 Roma, Italy

²Osservatorio Astronomico di Roma, Via Frascati 33, I-00040 Monteporzio, Italy

³Dep. of Astronomy and Astrophysics, The Pennsylvania State University, University Park, PA 16802, USA

⁴Osservatorio Astronomico di Bologna, Via Ranzani 1, I-40127 Bologna, Italy

⁵ASI Science Data Center, Via Galileo Galilei, I-00044 Frascati, Italy

⁶Istituto di Fisica Cosmica - CNR, Via Bassini 15, I-20121 Milano, Italy

⁷SISSA, Via Beirut 4, I-34014 Trieste, Italy

AGN model. In this framework the computation of the density of AGN has become an even more difficult task. In fact, it is not clear how to classify the sources and to take into account the selection biases introduced by the observation in the 2-10 keV range, where the absorption still play a relevant role.

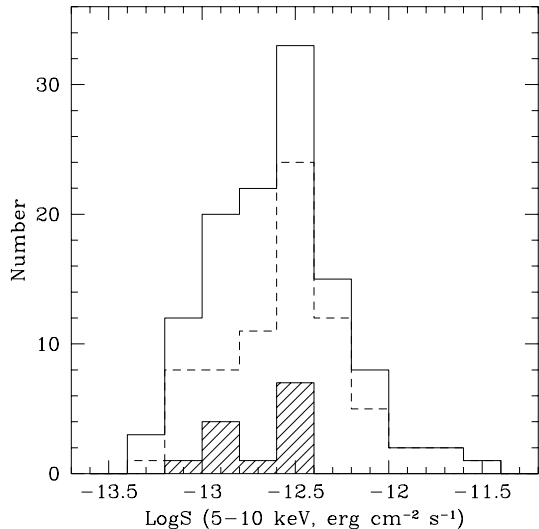


FIG. 1.— The flux distribution of the 118 sources from HELLAS used in this analysis (continuous line). The dashed line is the distribution of the 74 sources for which a spectroscopic identification campaign has been carried out (*empty* fields included). The distribution of the 13 sources for which we end up with an *empty* field is represented by the hatched histogram.

These recent deep surveys with *Chandra* and *XMM-Newton* have reached fluxes $\sim 5 \times 10^{-16}$ erg cm $^{-2}$ s $^{-1}$ (2-10 keV) in quite small areas (less than 1 deg 2). As a consequence these surveys are not able to provide statistical significant samples at brighter fluxes ($\sim 10^{-13}$ erg cm $^{-2}$ s $^{-1}$; 5-10 keV) where the density of sources is about 5/deg 2 (Fiore et al. 2001) and tens of square degrees are to be covered. Such data are necessary to provide large numbers of spectroscopic identified sources in a wide range of X-ray fluxes in order to cover as much as possible the L_X/z plane and hence to derive their X-ray luminosity function (LF).

In this paper we report the results of the spectroscopic identifications of one of such brighter samples. The X-ray sources have been detected by the *BeppoSAX*-MECS instruments in the 5-10 keV band in the framework of the High Energy LLarge Area Survey (HELLAS). Preliminary results have been presented in Fiore et al. (1999) and La Franca et al. (2001). The whole survey and the catalogue is described by Fiore et al. (2001). The data have been analyzed in the framework of the synthesis models for the X-ray background by Comastri et al. (2001), and the correlation with the soft X-rays has been investigated by Vignali et al. (2001).

In section 2 we describe our X-ray and optical observations. In section 3 we present an analysis of the evolution of AGN in the 2-10 keV band. Because of the reasons

previously described, the selection and definition of type 2/absorbed sources is still not clear, and thus we restricted our evolutionary studies to type 1 AGN only. The results are discussed in section 4.

2. THE SPECTROSCOPIC IDENTIFICATIONS

The spectroscopic follow up of the HELLAS sources has been carried out in a subsample enclosed in a region with $\delta < 79^\circ$, and outside $5^h < \alpha < 6.5^h$ and $17^h < \alpha < 20^h$. In this region the number of sources is 118 out of a total of 147. Their flux distribution is shown in Figure 1 and the sky coverage is shown in Figure 2 and listed in Table 1.

The *BeppoSAX* X-ray positions have an uncertainty of about 1-1.5 arcmin, the larger at larger off-axis distances. We have thus searched for optical counterparts having R magnitude brighter than 21.0 in a circular region of 1-1.5 arcmin of radius around the HELLAS positions (see below and section 3.1.1 for a discussion on the choice of this optical limit). In the case of large off-axis distances, the larger error-boxes (1.5') have been used. 25 sources have been identified with cross-correlation with existing catalogues (NED), and 49 have been investigated at the telescope. The total resulting sample of 74 sources has been built up in such a way that to a) randomly sample the flux distribution of the parent catalogue of 118 sources (see Figure 1), and b) to avoid possible biases introduced by the cross-correlation with existing catalogues (see appendix A for a detailed discussion).

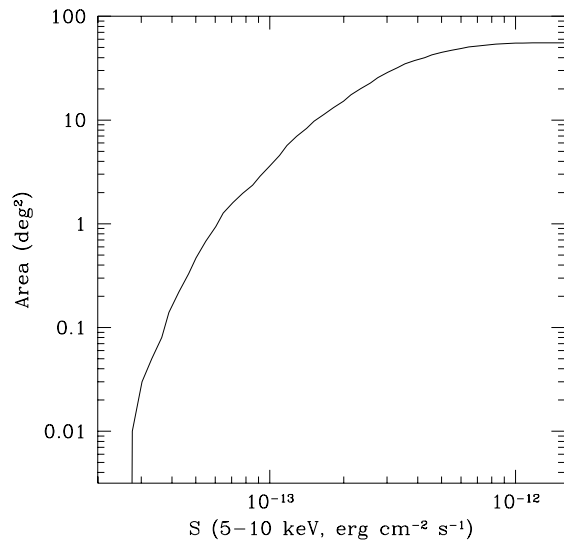


FIG. 2.— The sky coverage of the sample of 118 sources from HELLAS used in this analysis.

The follow-up observations have been carried out using the EFOSC2 at the 3.6m ESO telescope. Previously published identifications (Fiore et al. 1999) have been carried out with the RC spectrograph (RCSP) at the Kitt Peak 4m telescope, the FAST spectrograph at the Whipple 60'' telescope, and the Hawaii 88'' telescope. Long slit and multi object spectroscopy have been carried with resolution between 7 and 16Å. The reduction process used stan-

TABLE 2
OBSERVING LOG

Date	Telescope
1998 Dec 28: 3 nights	ESO/3.6m EFOSC2
1999 Jun 8: 3 nights	ESO/3.6m EFOSC2
2000 Jan 3: 3 nights	ESO/3.6m EFOSC2
2000 Jul 29: 3 nights	ESO/3.6m EFOSC2

dard MIDAS facilities (Banse et al. 1983). The raw data were sky-subtracted and corrected for pixel-to-pixel variations by division with a suitably normalized exposure of the spectrum of an incandescent source (flat-field). Wavelength calibrations were carried out by comparison with exposures of He-Ar, He, Ar and Ne lamps. Relative flux calibration was carried out by observations of spectrophotometric standard stars (Oke 1990). The campaign dates of the observations carried out at ESO are listed in Table 2.

We have divided the identified sources in AGN1, AGN2, galaxies with narrow emission lines showing moderate-to-high degree of excitation (ELG), BL Lac objects, clusters of galaxies and stars. AGN2 includes AGN1.5, AGN1.8 and AGN1.9. No distinction has been made between radio-loud and radio quiet objects. The radio properties of the HELLAS sources will be discussed in a forthcoming paper (P. Ciliegi, in preparation). The R-band magnitudes of these identifications have been pushed down to the limit of obtaining about less than 10% probability of having a spurious identification, due to chance coincidences, for each of the HELLAS sources (i.e. 90% reliability for the whole sample). For AGN1 we have chosen a limit of $R=21$ where the surface density is $\sim 60\text{-}70/\text{deg}^2$ (Zitelli et al. 1992). Tresse et al. (1996) found that 17% of galaxies with $z < 0.3$ host an emission line spectrum not typical of excitation from starburst (but typical of AGN2 activity), this percentage reduces to at minimum 8% if the maximum likely effect of absorption under the Balmer lines is taken into account. They also found that the galaxies having forbidden emission lines without being AGN2 are at least 36%. These objects are mainly starburst galaxies and low ionization narrow emission line galaxies (LINER). We will call here all these sources simply emission line galaxies (ELG). We have assumed roughly constant these percentages and thus chosen a limit of $R=19$ for AGN2 where the surface density of all galaxies is about $500/\text{deg}^2$ and consequently the expected density of AGN2 is $\sim 70\text{-}80/\text{deg}^2$. For ELG we have chosen a limit of $R=17.5$ where the surface density of all galaxies is about $160/\text{deg}^2$, and therefore the expected density of ELG is $\sim 60/\text{deg}^2$.

The classification of the narrow emission line galaxies has been carried out using standard line ratio diagnostics (Tresse et al. 1996). Some of the spectra showed H_α in emission and H_β having a) very small emission, or b) absent, or c) small absorption. Such spectra show however spectral features typical of strong-emission-line spectra such as $[\text{OII}]\lambda 3727$, $[\text{OIII}]\lambda 4959$, 5007, and $[\text{SII}]\lambda 6725$. In such cases the $[\text{OIII}]/H_\beta$ push the diagnostic ratio in

the locus of AGN2, but stellar absorption at H_β could be significant affecting the classification. Following Tresse et al. (1996), we have tested the classification under the assumption of a possible absorption of $\text{EW}=2\text{\AA}$ over H_β .

We have spectroscopically identified 36 out of the 49 HELLAS sources whose field has been investigated at the telescopes. For 13 sources we have found no optical counterparts brighter than the chosen magnitude limits (see discussion above). The astrometric accuracy of the new generation X-ray telescopes (*Chandra* and *XMM-Newton*) would probably allow an unambiguous identification of the counterparts of these HELLAS sources, but in the framework of this work these fields have been declared *empty*. These sources have harder X-ray spectra than the total sample. They have an average softness ratio of $\langle \frac{S-H}{S+H} \rangle = -0.5 \pm 0.3$ in comparison with the average value -0.1 ± 0.4 of the total sample of 118 sources, where S and H are the 1.3-4.5 keV the 4.5-10 keV counts, respectively (see Fiore et al. 2001). The absence of bright counterparts and the average harder X-ray spectrum favor the hypothesis that most of these sources preferably harbor absorbed AGN. If these sources correspond to optical "normal" galaxies, such as those observed by *Chandra* and *XMM-Newton* (see e.g. Fiore et al. 2000; Barger et al. 2001; Tozzi et al. 2001; Hornschemeier et al. 2001; Comastri et al. 2002), we would have not been able to properly identify them inside our error-boxes. However, our sample is statistically well defined, and from the number of empty fields we can directly derive an upper limit of $\sim 18\%$ (13/74) for the presence of these optical normal galaxies in our survey.

The list of the observed HELLAS sources with their most probable spectroscopic identification is shown in Table 3. 80% of our identifications are inside an error-box of 60 arcsecs. 2 bright galaxies ($R\sim 15\text{-}16$) are at a distance of about $110''$. The 13 empty fields are listed in Table 4. The optical spectra are shown in Figure 3; as a reference, a list of the most typical emission lines for AGN are over-plotted with the corresponding redshift. In Table 5 the EW, FWHM, FWZI in the observed frame of the most relevant emission lines are listed.

In total, 63% (74/118) of our HELLAS subsample has been searched for spectroscopic identification. 61 have been identified: 37 AGN1, 9 AGN2, 5 ELG, 6 Clusters, 2 BL Lac, 1 Radio Galaxy and 1 Star.

TABLE 3
IDENTIFIED HARD X-RAY SOURCES IN THE HELLAS CATALOGUE

BeppoSAX position				Optical position				Δ_{x_o}	Off _x	F _X 5-10 keV (1)	R	Spectr. ID	z		
RA (2000)		DEC		RA (2000)		DEC									
h	m	s	°	'	''	h	m	s	°	'	''				
00 26 36.5	-19 44 14	00 26 36.1	-19 44 16	7	13	3.4	18.1	AGN2	0.238						
00 27 09.9	-19 26 31	00 27 09.8	-19 26 14	18	6	1.8	17.7	AGN1	0.227 ^a						
00 45 49.6	-25 15 14	00 45 46.3	-25 15 50	59	24	3.3	17.5	AGN2	0.111						
01 21 56.8	-58 44 05	01 21 56.9	-58 44 42	37	16	2.6	16.8	AGN2	0.118						
01 34 33.3	-29 58 38	01 34 33.8	-29 58 16	24	6	0.9	18.0	AGN1	2.217						
01 35 30.2	-29 51 22	01 35 32.7	-29 52 02	53	8	0.9	17.7	AGN1	1.344						
01 40 08.9	-67 48 13	01 40 14.7	-67 48 54	53	8	2.8	12.4	Star	0.000						
02 42 01.8	+00 00 46	02 42 00.9	+00 00 22	29	10	1.5	18.6	AGN1	1.112†						
03 15 45.0	-55 29 26	03 15 47.5	-55 29 04	31	15	2.7	17.9	AGN1	0.464†						
03 17 32.4	-55 20 12	03 17 32.7	-55 20 26	14	21	4.1	17.5	AGN1	0.406†						
03 33 09.6	-36 19 40	03 33 12.2	-36 19 48	33	15	4.0	17.5	BLac	0.308†						
03 34 07.4	-36 04 22	03 34 07.5	-36 04 04	19	5	1.9	20.1	AGN1	0.904						
03 36 51.3	-36 15 57	03 36 54.0	-36 16 06	34	15	3.7	17.7	AGN1	1.537†						
04 37 14.5	-47 30 58	04 37 11.8	-47 31 48	57	16	2.7	17.3	AGN1	0.142						
04 38 47.9	-47 29 07	04 38 47.0	-47 28 02	67	20	4.7	20.5	AGN1	1.453						
06 46 39.3	-44 15 35	06 46 37.6	-44 15 34	19	17	4.3	16.6	AGN1	0.153						
07 21 29.6	+71 14 04	07 21 36.2	+71 13 24	52	8	0.8	17.7	AGN1	0.232†						
07 41 40.3	+74 14 58	07 41 50.0	+74 14 48	41	23	30.7	Clust.	0.216†						
07 43 09.1	+74 29 20	07 43 12.6	+74 29 36	22	7	6.0	16.4	AGN1	0.312†						
08 37 37.2	+25 47 49	08 37 37.1	+25 47 52	4	12	2.6	16.9	AGN1	0.077						
08 38 59.9	+26 08 14	08 38 59.2	+26 08 14	10	23	16.4	15.3	ELG	0.048						
10 32 15.8	+50 51 04	10 32 16.2	+50 51 20	18	10	3.1	15.9	AGN1	0.174						
10 54 19.8	+57 25 09	10 54 21.2	+57 25 44	38	13	2.6	18.5	AGN2	0.205†						
11 01 46.4	+72 26 11	11 01 48.8	+72 25 38	36	22	7.3	16.7	AGN1	1.460†						
11 02 37.2	+72 46 38	11 02 36.8	+72 46 40	3	21	7.9	15.1	AGN1	0.089†						
11 06 14.0	+72 43 16	11 06 16.1	+72 44 14	59	9	1.7	18.5	AGN1	0.680†						
11 18 11.9	+40 28 33	11 18 13.8	+40 28 38	23	4	0.8	18.7	AGN1	0.387						
11 18 46.2	+40 27 39	11 18 48.7	+40 26 48	59	5	1.4	18.5	AGN1	1.129						
12 04 07.6	+28 08 31	12 04 04.0	+28 07 24	82	16	5.1	Clust.	0.167†						
12 17 50.3	+30 07 08	12 17 52.1	+30 07 02	25	20	3.5	14.0	BLac	0.237†						
12 18 55.0	+29 58 12	12 18 52.5	+29 59 02	59	13	2.0	18.6	AGN2	0.176						
12 19 45.7	+47 20 43	12 19 52.3	+47 20 58	69	8	1.2	19.3	AGN1	0.654†						
12 22 06.8	+75 26 17	12 22 07.0	+75 26 18	2	7	2.5	Clust.	0.240†						
12 40 26.0	-05 13 20	12 40 27.8	-05 14 02	50	12	3.1	18.8	AGN1	0.300						
12 40 29.6	-05 07 46	12 40 36.4	-05 07 52	102	17	1.9	15.2	ELG	0.008						
13 04 38.2	-10 15 47	13 04 35.6	-10 15 48	39	6	1.4	20.1	AGN1	2.386						
13 05 32.3	-10 32 36	13 05 33.0	-10 33 20	45	22	19.3	14.9	AGN1	0.278†						
13 36 34.3	-33 57 48	13 36 39.0	-33 57 58	60	22	3.2	10.5	RadioG.	0.013†						
13 42 59.3	+00 01 38	13 42 56.5	+00 00 58	59	21	3.2	18.7	AGN1	0.804†						
13 48 20.8	-30 11 06	13 48 19.5	-30 11 56	52	14	2.2	15.3	AGN2	0.128						
13 48 45.4	-30 29 37	13 48 44.7	-30 29 46	13	14	5.1	17.1	AGN1	0.330						
13 50 09.4	-30 19 55	13 50 15.4	-30 20 10	80	11	5.1	16.5	ELG	0.074						
13 53 54.6	+18 20 33	13 53 54.4	+18 20 16	18	18	6.8	17.3	AGN1	0.217						
14 17 12.5	+24 59 29	14 17 18.8	+24 59 30	86	13	0.7	19.5	AGN1	1.057†						
14 18 31.1	+25 11 07	14 18 31.2	+25 10 50	17	9	6.1	Clust.	0.240†						
15 19 39.9	+65 35 46	15 19 33.7	+65 35 58	41	14	9.4	14.4	AGN2	0.044						
15 28 47.3	+19 39 10	15 28 47.7	+19 38 54	18	5	1.6	20.3	AGN1	0.657 ^b						
16 26 59.9	+55 28 21	16 26 59.0	+55 27 24	57	11	12.1	Clust.	0.130†						
16 34 11.8	+59 45 29	16 34 18.5	+59 45 44	53	3	0.8	19.0	AGN2	0.341 ^c						
16 49 57.9	+04 53 33	16 50 00.0	+04 54 00	42	20	9.5	Clust.	0.154†						
16 50 40.1	+04 37 17	16 50 42.7	+04 36 18	71	25	12.2	14.6	AGN2	0.031						
16 52 38.0	+02 22 18	16 52 37.5	+02 22 06	14	5	0.7	20.7	AGN1	0.395						
20 42 47.6	-10 38 31	20 42 53.0	-10 38 26	80	21	5.3	17.9	AGN1	0.363						
20 44 34.8	-10 27 34	20 44 34.8	-10 28 08	35	15	2.0	17.7	AGN1	2.755						
22 26 30.3	+21 11 57	22 26 31.5	+21 11 38	26	14	3.9	17.6	AGN1	0.260						
23 15 36.4	-59 03 40	23 15 46.8	-59 03 14	85	8	2.0	11.2	ELG	0.044†						
23 19 22.1	-42 41 50	23 19 32.0	-42 42 28	116	21	5.7	16.5	ELG ^d	0.101						
23 27 28.7	+08 49 30	23 27 28.7	+08 49 26	4	7	0.5	18.5	AGN1 ^e	0.154						
23 29 02.4	+08 34 39	23 29 05.8	+08 34 16	56	20	2.9	20.3	AGN1	0.953						
23 31 55.6	+19 38 34	23 31 54.3	+19 38 36	19	17	3.7	18.8	AGN1	0.475						
23 55 53.3	+28 36 06	23 55 54.3	+28 35 58	16	12	4.2	17.9	AGN1	0.731†						

NOTE.— (1) 10^{-13} erg cm⁻² s⁻¹; † From cross-correlation with existing catalogues; ^a) From Colafrancesco et al. (2000); ^b) From Gorosobel et al. (1998), misidentified in Fiore et al. 2000; ^c) Wrong coordinates and magnitudes in Fiore et al. (1999); ^d) Also possible AGN1: H_β has a rest frame FWHM~1000 Km/s; ^e) On its own spectrum, H_β has a rest frame FWHM~1500 Km/s

TABLE 4
EMPTY FIELDS IN THE HELLAS CATALOGUE

<i>BeppoSAX</i> position						F_X
RA (2000)			DEC			5-10 keV
<i>h</i>	<i>m</i>	<i>s</i>	°	'	''	(10^{-13} erg cm $^{-2}$ s $^{-1}$)
01	34	28.6	-30	06	04	1.33
01	34	49.6	-30	02	34	0.71
09	46	05.3	-14	02	59	2.82
09	46	32.8	-14	06	16	3.22
13	04	24.3	-10	23	53	1.28
13	04	45.1	-05	33	37	1.26
13	48	24.3	-30	25	47	3.15
14	11	58.7	-03	07	02	3.93
22	03	00.5	-32	04	18	2.83
22	31	49.6	+11	32	08	1.94
23	02	30.1	+08	37	06	2.67
23	02	36.2	+08	56	42	3.17
23	16	09.8	-59	11	24	1.32

NOTE.—Within 1 arcmin there are no AGN1 down to $R=21$, no AGN2 down to $R=19$ and no ELG down to $R=17.5$.

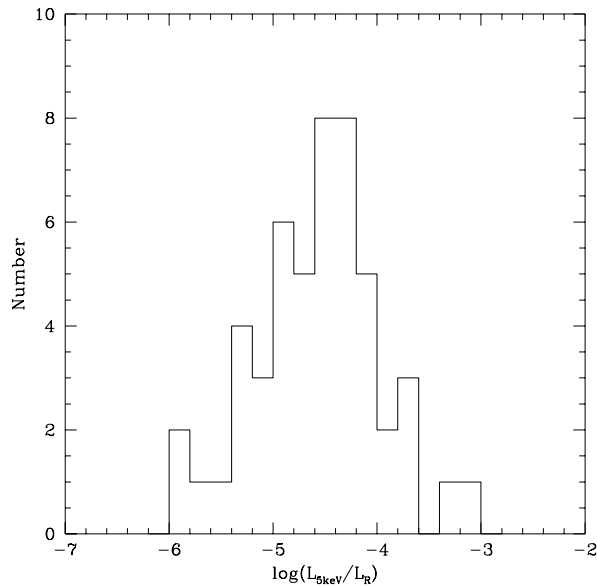


FIG. 4.— The histogram of the $\text{Log}(L_{5 \text{ keV}}/L_R)$ ratio for a sample of 50 (25 X-ray selected and 25 optically selected) AGN1 (see text). We fitted the distribution with a Gaussian having mean -4.58 and standard deviation 0.61. This distribution has been assumed as representative of the whole population of type 1 AGNs at any redshift and luminosity, and used to compute the fraction of AGN1 fainter than $R=21$ missed from the optical spectroscopic identifications of the HELLAS sample.

3. ANALYSIS ON THE EVOLUTION OF AGN1

Because of the difficulties previously described in quantifying all the selection biases in building up samples of type 2 (and/or absorbed) AGN, we have decided to limit our evolutionary analysis to AGN1 only. See appendix A for a discussion on the absence of substantial biases on our sample of AGN1. We have assumed $H_0=50$ km/s/Mpc and either the $(\Omega_m, \Omega_\lambda)=(1.0, 0.0)$ or the $(\Omega_m, \Omega_\lambda)=(0.3, 0.7)$ cosmologies. We have computed the 2-10 keV luminosity for AGN1 assuming a typical spectral energy distribution as computed by Pompilio, La Franca, & Matt (2000), which assumes a power slope in energy with index $\alpha=0.9$ ($\frac{dF}{dE} \propto E^{-\alpha}$) and takes into account the reflection. This spectrum is roughly approximated by a single power $\alpha=0.6$ in the range 2-50 keV (i.e. up to $z=4$). This is in agreement with the average slope of the spectra of AGN1 from the HELLAS sample (Vignali et al. 2001).

3.1. The data

3.1.1. The completeness of the sample of AGN1 from HELLAS

As our spectroscopic identifications are limited to magnitudes brighter than $R = 21$, in order to estimate the density of AGN1, we have evaluated which is their completeness in our sample. We have assumed that all AGN1 follow the same distribution of the ratio of the 5 keV to R-band optical luminosity $\text{Log}(L_{5 \text{ keV}}/L_R)$ without dependencies on luminosity and/or redshift. We have estimated the relationship between optical and hard X-ray luminosity for AGN1 as follow. We selected a mixed sample of both 25 optical and 25 hard X-ray selected type 1 AGN, mostly in the redshift range $0 < z < 2$, from Mineo et al. (2000), George et al. (2000) and Akiyama et al. (2000). The 25 optically selected AGN1 have an average $\text{Log}(L_{5 \text{ keV}}/L_R)$ ratio of -4.78 with a standard deviation of 0.59, while the

25 X-ray selected AGN1 have an average $\text{Log}(L_{5 \text{ keV}}/L_R)$ ratio of -4.38 with a standard deviation of 0.58. In Figure 4 the histogram of the ratio of 5 keV and R-band optical luminosity of the total sample of 50 AGN1 at $z=0$ is shown. We fitted the distribution with a Gaussian having mean -4.58 and standard deviation 0.61. We have estimated that with this distribution, a limit of $R = 21$ corresponds to only 1 AGN1 lost from our HELLAS survey, and consequently we can say that a limit of $R = 21$ assure a high level of completeness for the identification of AGN1 at the fluxes of our HELLAS survey. At variance, as already discussed, our HELLAS identification programme is biased against absorbed type 2 sources which probably harbor in the 13 empty fields found.

Although the incompleteness for AGN1 in the HELLAS sample is quite low, during the computation of the LF of AGN1, we have estimated the correct area coverage for our survey by multiplying the area coverage corresponding to each point of the L_X/z plane for: a) the spectroscopic completeness of the HELLAS sample (74/118), and b) the fraction of found AGN1 as a function of z , as described before.

3.1.2. The other samples

In order to increase the statistical significance of our analysis, the HELLAS data have been combined to other hard X-ray samples of AGN1 identified by Grossan (1992), Boyle et al. (1998), and Akiyama et al. (2000).

The sample of Grossan (1992) consists of 84 AGN1 and 12 AGN2 detected by *HEAO1*, predominantly at low redshift $z < 0.3$. The sample covers an area of 26919 deg² down to a flux limit of 1.8×10^{-11} erg cm⁻² s⁻¹. The quoted fluxes at 5 keV have been converted to fluxes in the 2-10 keV assuming $\alpha = 0.6$.

The sample of Boyle et al. (1998) consists of 12 AGN1 and 6 AGN2 detected by *ASCA*. 2-10 keV counts have been converted to fluxes with a count-rate-to-flux conversion factor of 5.8×10^{-11} erg cm⁻² s⁻¹/count, assuming $\alpha = 0.6$ (Georgantopoulos et al., 1997). The sky coverage has been taken from Georgantopoulos et al. (1997, see their figure 1).

The sample of Akiyama et al. (2000) consists of 25 AGN1, 5 AGN2, 2 clusters, 1 star and 1 unidentified source. The sources have been detected by *ASCA*. In order to convert the counts of the sky coverage presented in their Table 1, a conversion has been applied assuming that 1 count corresponds to 0.9×10^{-13} erg cm⁻² s⁻¹ in the 2-10 keV band for an X-ray source with a slope $\alpha=0.6$.

A total of 158 AGN1 have been used in the redshift range $0 < z < 3$. Their luminosity-redshift distribution is shown in Figure 5. In this distribution a gap between the sample of Grossan from *HEAO1* and the other fainter samples from *ASCA* and *BeppoSAX* is evident. This is because surveys at fluxes in the range 10^{-12} - 10^{-11} erg cm⁻² s⁻¹ in the 2-10 keV energy band where some hundreds of deg² need to be covered are still missing. These surveys are in program with *XMM-Newton* (see e.g. Barcons et al. 2001).

3.2. The method

The best-fit parameters for the 2-10 keV LF and its cosmological evolution have been derived by minimization of

the χ^2 computed by comparison of the observed and expected number of AGN1 in 6×3 bins in the L_X/z plane. The adopted luminosity/redshift grid was: 6 $\text{Log}L_X$ bins, with $\Delta \text{Log}L_X=1$ in the range 42.2-48.2, and 3 redshift bins (0.0-0.2, 0.2-1.0, 1.0-3.0). Table 6 summarizes the results for a number of different models. The errors quoted for the parameters are 68% (1σ) confidence intervals. They correspond to variations of $\Delta\chi^2=1.0$, obtained perturbing each parameter in turn with respect to its best-fit value, and looking for a minimization with the remaining parameters free to float. The fitted LF have been tested with the 2D Kolmogorov-Smirnov (2DKS) test. Two different functional forms have been used. Following Ceballos and Barcons (1996) and Boyle et al. (1998), we used the pure luminosity evolution (PLE) for the AGN1 LF. We also used the luminosity dependent density evolution (LDDE) model similar to the one fitted in the soft X-rays by Miyaji et al. (2000).

The local ($z=0$) AGN1 LF used for the PLE model has been represented by a two-power-law:

$$\begin{aligned} \frac{d\Phi(L_X)}{dL_X} &= A(L_X^{*(\gamma_1-\gamma_2)})L_X^{-\gamma_1} & : L_X \leq L_X^*(z=0), \\ \frac{d\Phi(L_X)}{dL_X} &= AL_X^{-\gamma_2} & : L_X > L_X^*(z=0), \end{aligned}$$

where L_X is expressed in units of 10^{44} erg s⁻¹. A standard power-law luminosity evolution model was used to parameterize the cosmological evolution of this LF: $L_X^*(z) = L_X^*(0)(1+z)^k$.

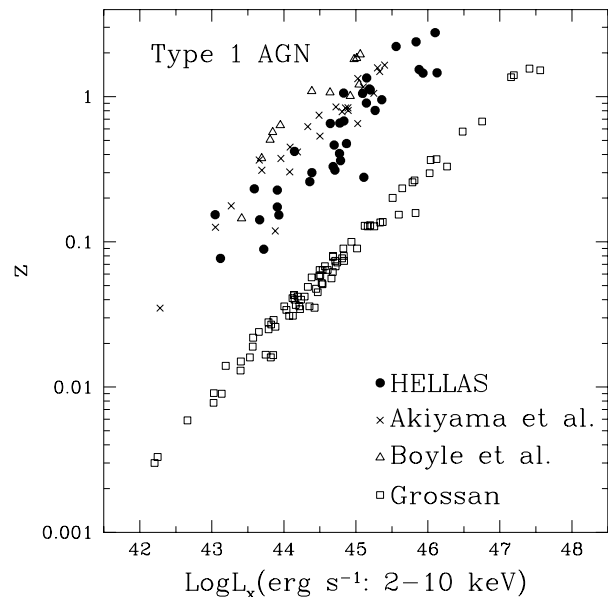


FIG. 5.— The luminosity/redshift distribution for all the 158 AGN1 used to compute the hard X-ray 2-10 keV luminosity function. $H_0=50$ km/s/Mpc and $(\Omega_m, \Omega_\Lambda)=(1.0, 0.0)$ have been assumed. It includes 37 AGN1 from HELLAS, 84 AGN1 from Grossan (1992), 12 from Boyle et al. (1998) and 25 from Akiyama et al. (2000).

In the case of the LDDE model, as an analytical expression of the present day ($z=0$) luminosity function, we used the smoothly connected two power-law form:

$$\frac{d\Phi(L_x, z=0)}{d\text{Log}L_x} = A[(L_x/L_*)^{\gamma_1} + (L_x/L_*)^{\gamma_2}]^{-1}.$$

The description of the evolution is given by a factor $e(L_x, z)$ such that:

$$\frac{d\Phi(L_x, z)}{d\text{Log}L_x} = \frac{d\Phi(L_x, z=0)}{d\text{Log}L_x} \times e(L_x, z),$$

where

$$e(L_x, z) = \begin{cases} (1+z)^{\max(0, p1-\alpha \text{Log}[L_a/L_x])} & (z \leq z_c; L_x < L_a) \\ (1+z)^{p1} & (z \leq z_c; L_x \geq L_a) \\ e(L_x, z_c) [(1+z)/(1+z_c)]^{p2} & (z > z_c). \end{cases}$$

The parameters are defined as in Miyaji et al. (2000). In particular, α is proportional to the decrease of the density evolution of the faint objects. In this parameterization of the LF L_x is expressed in units of erg s^{-1} . In both models the LF has been computed for luminosities brighter than $\text{Log}L_{2-10\text{keV}}=42.2$. Using this parameterization, for $(\Omega_m, \Omega_\Lambda)=(1.0, 0.0)$, a fit was done by keeping fixed the parameters $z_c=1.55$ (the redshift at which the evolution stops), $\alpha=2.5$, and the ratio $L_a/L_* = 10^{0.42}$ to the value found by Miyaji et al. (2000) for AGN1 only (their LDDE1 model) in the soft X-rays, and leaving all the remaining parameters (the two slopes γ_1 and γ_2 , the break luminosity L_* , and the speed of the density evolution $p1$) free to vary. In the case of an $(\Omega_m, \Omega_\Lambda)=(0.3, 0.7)$ Universe, as the fit for AGN1 only from Miyaji et al. (2000) was not available, their parameters from the fit for all AGNs (AGN1+AGN2) have been used: $z_c=1.58$, $\alpha=2.6$, $L_a/L_* = 10^{0.65}$.

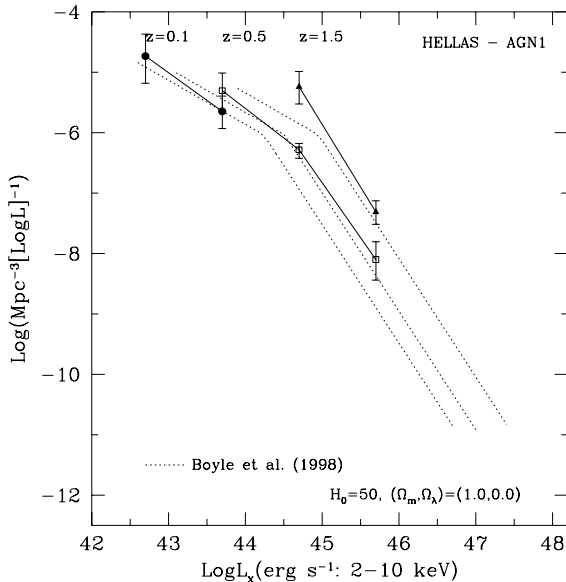


FIG. 6.— The luminosity function of the 37 HELLAS AGN1. As a reference, the dotted lines show the previously estimated luminosity function in the 2-10 keV from Boyle et al. (1998).

3.3. Results

3.3.1. The LF in the $(\Omega_m, \Omega_\Lambda)=(1.0, 0.0)$ universe

We started our computation of the LF in an $(\Omega_m, \Omega_\Lambda)=(1.0, 0.0)$ cosmology. Previous estimates of the shape and evolution of the LF of AGN1 in the 2-10 keV range are from Ceballos and Barcons (1996), and Boyle et al. (1998). Boyle et al. (1998) combined the local sample of 84 AGN1 observed by *HEAO1* from Grossan (1992) with a fainter sample of 12 AGN1 observed by *ASCA* (see their distribution in the L_x - z plane in Figure 4). They found that the 2-10 keV AGN X-ray LF is best represented by a two-power-law function evolving according to a pure luminosity evolution (PLE) model: $L_x(z) \propto (1+z)^{2.00}$ (see model 0 in Table 6).

In Figure 6 the LF from only the 37 AGN1 from HELLAS in three redshift intervals ($0.0 < z < 0.2$, $0.2 < z < 1.0$, and $1.0 < z < 3.0$) is shown. For the sake of comparison, the best-fit LF from Boyle et al. (1998) is also shown. The data have been represented by correcting for evolution within the redshift bins as explained in La Franca & Cristiani (1997). The error bars in the figures are based on Poisson statistics at the 68% confidence level.

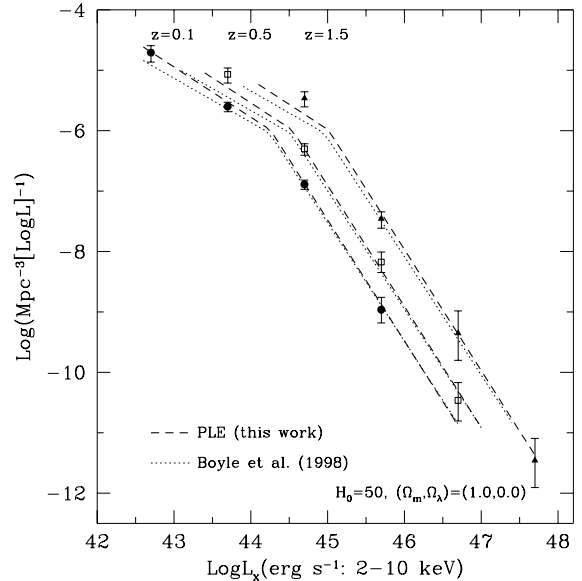


FIG. 7.— The LF of the total sample of 158 AGN1 including the 37 AGN1 from HELLAS, 84 from Grossan (1992), 12 from Boyle et al. (1998) and 25 from Akiyama et al. (2000). The excess of faint AGN1 at high redshift is even more evident than in the previous figure. The dotted line is the PLE fit by Boyle et al. (1998). The dashed line is our best PLE fit (see Table 6).

The data are in rough agreement with the previous estimate of Boyle et al. (1998), but show an excess of faint AGN1 at redshift larger than $z \sim 1.0$. This feature is still present after combining our data with the other AGN1 samples from Grossan (1992), Boyle et al. (1998), and Akiyama et al. (2000) (Figure 7).

TABLE 6
THE 2-10 KEV AGN LF PARAMETERS

Model	Ω_m, Ω_λ	γ_1	γ_2	$\text{Log}L^*$	k or $p1$	z_{cut}	A^a	$Prob$	f_{XRB}^1
0) PLE from Boyle	1.0,0.0	1.73	2.96	44.16	2.00	...	8.2×10^{-7}	0.04 ^b	24
1) PLE	1.0,0.0	1.83	3.00	44.17	2.12	...	9.8×10^{-7}	0.22	35
2) PLE with z_{cut}	1.0,0.0	1.87	3.03	44.17	2.52	1.39	8.9×10^{-7}	0.31	34
3) LDDE	1.0,0.0	0.68	2.02	44.03	4.66	1.55 ^c	2.0×10^{-6} ^d	0.47	40
4) PLE	0.3,0.7	1.93	2.97	44.24	2.22	...	8.7×10^{-7}	0.47	56
5) PLE with z_{cut}	0.3,0.7	1.94	2.97	44.24	2.26	2.38	8.7×10^{-7}	0.70	54
6) LDDE	0.3,0.7	0.69	1.95	43.96	4.56	1.58 ^c	2.3×10^{-6} ^d	0.77	60
7) LDDE softX	1.0,0.0	0.62 ^c	2.25 ^c	44.13	5.40 ^c	1.55 ^c	1.4×10^{-6} ^{c,d}	0.11	48
68% confidence errors		+0.12 -0.16	+0.11 -0.09	+0.13 -0.15	+0.13 -0.14	+0.56 -0.25	8%		

NOTE.— (1) % of the XRB: $I_{2-10} = 1.95 \times 10^{-11} \text{ erg cm}^{-2} \text{ s}^{-1} \text{ deg}^{-2}$ (Chen, Fabian and Gendrau 1997)
(a) $\text{Mpc}^{-3}(10^{44} \text{ erg s}^{-1})^{-1}$; (b) χ^2 probability; (c) fixed; (d) $\text{Mpc}^{-3}(\text{erg s}^{-1})^{-1}$.

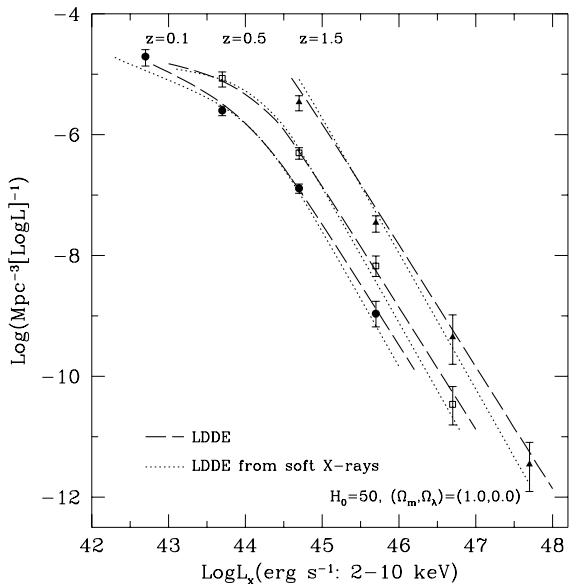


FIG. 8.— The luminosity function of AGN1 fitted with the LDDE model (dashed line). The soft X-ray LF (Miyaji et al. 2000) is also shown (dotted line), with the assumption $\text{Log}L_{2-10\text{keV}} = \text{Log}L_{0.5-2\text{keV}} + 0.33$ (see text).

As already discussed, these samples all together collect 158 AGN1. These data have a χ^2 probability of 0.04 to be drawn from a PLE model such as that computed by Boyle et al. (1998) (model 0 in Table 6). We did not use the 2DKS as this test is not appropriate in this case: it uses the cumulative distributions in the L_X/z plane regardless of the normalization of the LF. Our best-fit to the data with a PLE model found a LF with similar slopes and break luminosity as that one of Boyle et al. (1998) but with a slightly larger evolution ($k = 2.12^{+0.13}_{-0.14}$ instead of $k = 2.00^{+0.16}_{-0.22}$), and a significantly 20(+9) % larger normal-

ization (the normalization has a Poisson uncertainty of 8%. See model 1 in Table 6).

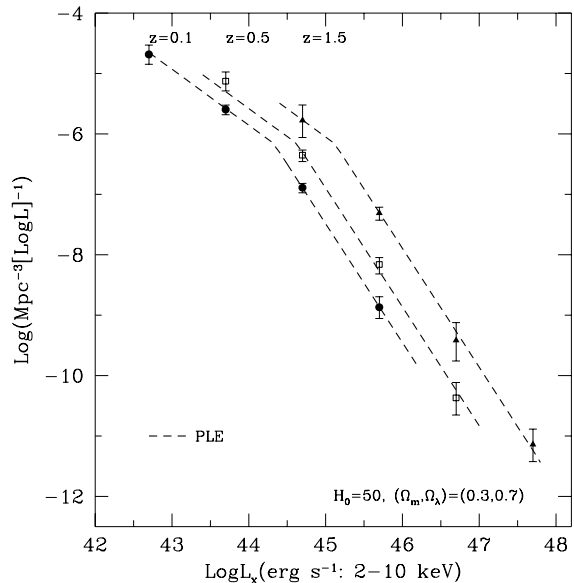


FIG. 9.— The luminosity function in the $(\Omega_m, \Omega_\lambda) = (0.3, 0.7)$ universe fitted by our PLE model (see Table 6).

Our larger values of the evolution parameter k and normalization A are originated by the necessity of better fitting the observed higher density of faint AGN1 at high redshift. The 2DKS test gives a probability of 0.22 for this fit (see Table 6). A even better probability of 0.31 is obtained if a stop in the evolution is applied at redshift $z_{cut} = 1.39$ (model 2 in Table 6) and a larger evolution ($k = 2.52$) is used.

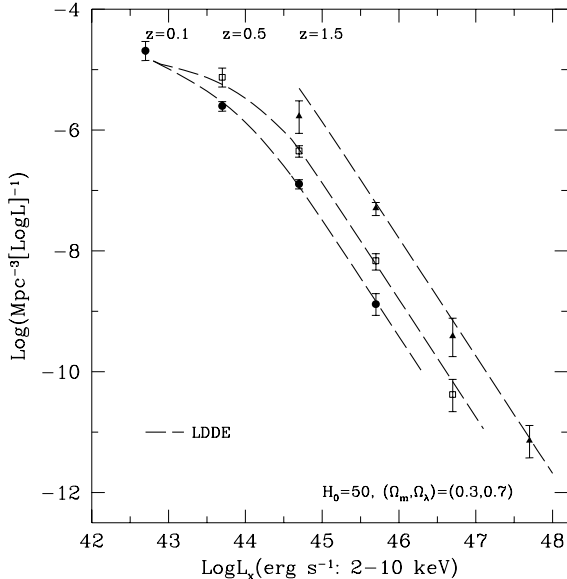


FIG. 10.— The luminosity function in the $(\Omega_m, \Omega_\lambda)=(0.3, 0.7)$ universe fitted by the LDDE model (see text and Table 6).

Although our fits are already statistically adequate, our PLE models do not fully describe an over-density of faint AGN1 which is observed at high redshift. The data are not sufficiently faint to properly probe this part of the LF, but as this feature is similar to what observed in the soft X-rays (Miyaji et al. 2000), we tried to obtain a even better fit of the data, by using the luminosity dependent density evolution (LDDE) model similar to the one fitted in the soft X-rays, as described in the previous section. This model differentiates from the PLE especially in the faint part of the LF, at luminosities lower than L_* . In this part of the LF the density evolution decreases in proportion to the faintness of the objects. As our data just start to probe the part of the LF which is fainter than L_* , we cannot expect to find directly a fit to all the parameters of the LDDE model to our data, and we limited our analysis to a check of the compatibility (with limited changes) of the LDDE parameters found by Miyaji et al. (2000) to our data. With this model we found the best-fit to our data (model 3: LDDE, Figure 8) by keeping fixed the parameters describing the stop in the evolution ($z_c=1.55$), and the dependence on luminosity of the density evolution ($\alpha=2.5$) to the value found by Miyaji et al. (2000) for AGN1 only, and leaving all the remaining parameters free to vary (see section 3.2). The 2DKS test gives, for this model, a probability of 0.47.

3.3.2. The $(\Omega_m, \Omega_\lambda)=(0.3, 0.7)$ universe

If an $(\Omega_m, \Omega_\lambda)=(0.3, 0.7)$ cosmology is assumed, the PLE models provide an ever better representation of the data in comparison with what found in the $(\Omega_m, \Omega_\lambda)=(1.0, 0.0)$ Universe (see Figure 9). The 2DKS probability is 0.70 and 0.47, with and without the introduction of the z_{cut} parameter, respectively. In this case even the simple PLE model obtain a quite good fit of the data, and the introduction of the z_{cut} parameter is necessary to stop the evolution only

at redshifts larger than 2.4. However our data contain not enough AGN1 at redshift larger than 2 in order to obtain an accurate measure of the z_{cut} parameter (see Figure 4), therefore the errors in this parameter are quite large. Also the LDDE model obtain a satisfactory fit of the data (see Figure 10).

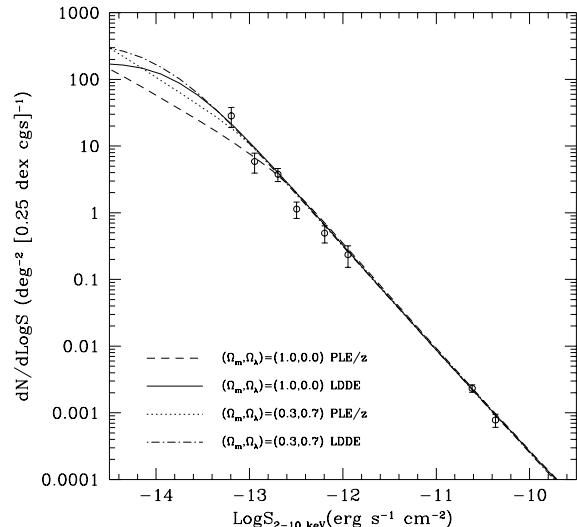


FIG. 11.— The differential counts of the type 1 AGN used in the estimate of the luminosity function. The models are explained in Table 6.

4. DISCUSSION AND CONCLUSIONS

Thanks to the identification of 61 sources of the HELLAS sample we have been able to double the number of hard X-ray AGN1 available for statistical analysis at fluxes in the range $f_{2-10keV} \sim 10^{-13.5}-10^{-12}$ erg cm $^{-2}$ s $^{-1}$. In total we can use 74 AGN1 at these fluxes (37 from HELLAS), which combined with the local sample of Grossan have allowed to show directly the shape of the LF of AGN1 as function of redshift and measure its evolution.

The PLE models provide satisfactory fits of the data both in the $(\Omega_m, \Omega_\lambda)=(1.0, 0.0)$ and in the $(\Omega_m, \Omega_\lambda)=(0.3, 0.7)$ cosmologies. Our estimate of the LF in the $(\Omega_m, \Omega_\lambda)=(1.0, 0.0)$ has a significantly larger normalization in comparison to the previous measure from Boyle et al. (1998).

The data start to probe in the hard X-rays the faint part of the LF where the excess of density of AGN1 has been observed in the soft X-rays, justifying the implementation of the LDDE models. However, in both cosmologies, the statistic is not significant enough to distinguish between the PLE and LDDE models (see Table 6). In fact, in the prediction of the differential counts of AGN1 shown in Figure 11, the models differentiates at fluxes fainter than $f_{2-10keV} \sim 10^{-13}$ erg cm $^{-2}$ s $^{-1}$, where the statistic is still poor. The new upcoming fainter surveys from *Chandra* and *XMM-Newton* will easily test which model is correct.

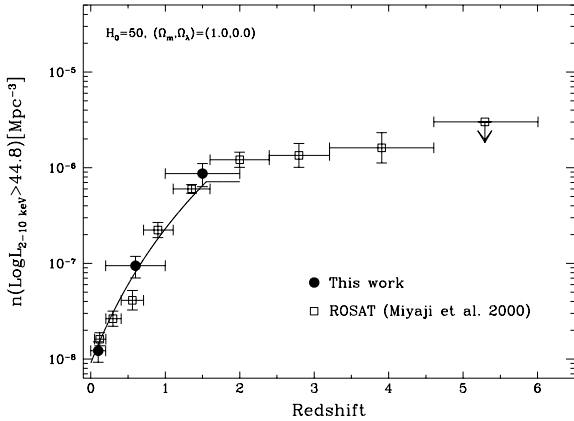


FIG. 12.— The evolution of the density of type 1 AGN having $\text{Log}L_X(2-10 \text{ keV}) > 44.8$ as a function of redshift. The soft X-ray data from Miyaji et al. (2000) have been over-plotted assuming a slope $\alpha = 0.6$, which corresponds to a limit $\text{Log}L_X(0.5-2 \text{ keV}) > 44.5$. The continuous line are the predictions of our LDDE model.

In Table 6 the percentages of the contribution to the 2-10 keV X-ray background are shown. The X-ray background has been computed integrating the LF up to $z = 3.5$ for $L_X > 10^{42} \text{ erg/s}$. At variance with the results of 24% obtained from the evolution of the LF derived by Boyle et al. (1998), our models reproduces from $\sim 35\%$ up to $\sim 60\%$ of the XRB. We used $I_{2-10} = 1.95 \times 10^{-11} \text{ erg cm}^{-2} \text{ s}^{-1} \text{ deg}^{-2}$ from Chen, Fabian and Gendreau (1997). The highest percentages would probably imply that part of the absorbed population necessary to reproduce the XRB is already included in the AGN1 at high redshift. However, more detailed analysis of this issue are beyond the scope of this paper. The percentages would decrease if a value of $I_{2-10} = 2.35 \times 10^{-11} \text{ erg cm}^{-2} \text{ s}^{-1} \text{ deg}^{-2}$ from Vecchi et al. (1999) is assumed.

It is interesting to notice that AGN1 in the 2-10 keV range show an evolution up to $z \sim 2$ which is fairly well compatible with what observed in the soft X-rays. In fact we found a good fit of the data in the $(\Omega_m, \Omega_\lambda) = (1.0, 0.0)$ Universe if we assume exactly the same parameters found in the soft X-rays by Miyaji et al. (2000) for AGN1, by only looking for a fit with the break luminosity L_* (model 7 in Table 6). Miyaji et al. (2000) found $\text{Log}L_* = 43.78$. The value L_* found by our fit in the 2-10 keV band is $\text{Log}L_* = 44.13$. This luminosity difference implies an X-ray spectrum for AGN1 with slope $\alpha = 0.6$, which is the same slope used in our computation of the LF. We note however that Miyaji et al. (2000) used a slope $\alpha = 1.0$ in their computations of the soft X-ray LF. Therefore, taken at a face value, the match between the soft and hard X-rays LFs implies that AGN1 have a broad band concave spectrum getting steeper going toward lower energies. As already discussed in the previous section, the $(\Omega_m, \Omega_\lambda) = (0.3, 0.7)$ cosmology for AGN1 alone has not been analyzed by Miyaji et al. (2000).

The agreement of the evolution measured in the soft and hard X-rays is also shown in Figure 12, where the evolution of the density of AGN1 brighter than $\text{Log}L_{2-10 \text{ keV}} = 44.8$ is shown. The soft X-ray data from Miyaji et al. (2000) have been over-plotted assuming a slope $\alpha = 0.6$, which corresponds to a limit $\text{Log}L_X(0.5-2 \text{ keV}) > 44.5$. The continuous line are the predictions of our LDDE model for $(\Omega_m, \Omega_\lambda) = (1.0, 0.0)$.

Based on observations collected at the European Southern Observatory, Chile, ESO N°: 62.P-0783, 63.O-0117(A), 64.O-0595(A), 65.O-0541(A). This research has made use of the NASA/IPAC Extragalactic Database (NED) which is operated by the Jet Propulsion Laboratory, California Institute of Technology, under contract with the National Aeronautics and Space Administration. This research has been partially supported by ASI contract ARS-99-75, MURST grants Cofin-98-02-32, Cofin-99-034, Cofin-00-02-36 and a 1999 CNAA grant.

APPENDIX

THE BIASES INTRODUCED BY THE CROSS CORRELATIONS WITH CATALOGUES

As already described, 25 sources have been identified by cross-correlation with existing catalogues. However, as the sample is not fully spectroscopic identified, the cross-correlation with the existing catalogues could alter the average characteristics (fluxes, percentages of classes of counterparts, etc.) of the subsample of identified sources. Namely, the subsample could not be representative of the whole sample.

Let's explain this with an example. In an ideal sample of 50 AGN1 and 50 AGN2 a random identification of a subsample of 40 sources will identify about 50% AGN1 and 50% AGN2 according to sampling errors. But if a cross-correlation is first made with a catalogue of only AGN1 (let say 30) and later only 10 sources are randomly identified, the fraction of AGN1 in the total identified subsample of 40 sources will be artificially increased (they will be at minimum 75%). Our subsample is risking the same sort of bias, and we wish to quantify it.

A Kolmogorov-Smirnov (KS) two-sample test gives a 9% probability that the X-ray flux distribution of the 25 sources identified through the cross-correlation with catalogues belong to the same parent population of the total sample of 118 sources. Although not significant, this low probability is due to the average slightly brighter fluxes of the cross-correlated subsample ($\langle \text{Log}F_{5-10 \text{ keV}} \rangle = -12.4 \pm 0.4$) in comparison to the total sample ($\langle \text{Log}F_{5-10 \text{ keV}} \rangle = -12.6 \pm 0.3$). We have thus tried to populate the faintest bins during the observing runs at the telescope, and, indeed, the KS test gives a 66% probability that the whole subsample of the 74 identified sources (included the empty fields) belong to the same parent population of the total sample of 118 sources (see Figure 1).

In this way, our observing runs at the telescope have recovered the possible alteration on the fraction of classes of sources which are identified. As the catalogues used for the cross correlation are mainly populated by AGN1 (we used

NED), their fraction in our sample, as explained before, could be artificially increased. AGN1 are 14 out of the 25 cross-correlated sources (56%). The fraction of AGN1 is, as expected (but not significantly), lower for the sources observed at the telescope: 23 out of the 49 (47%). The two values are not statistically distinguishable from the observed fraction 50% of AGN1 in the whole sample, which we thus consider representative of the whole HELLAS sample.

REFERENCES

- Akiyama, M. et al., 2000, ApJ, 532, 700
 Antonucci, R., 1993, ARA&A, 2105, 1308
 Baldi A., Molendi S., Comastri A., Fiore F., Matt G., Vignali C. 2001, ApJ, in press, preprint (astro-ph/0108514)
 Banse, K., Crane, P., Grosbol, P., Middleburg, F., Ounnas, C.; Ponz, D., Waldthausen, H. 1983, The Messenger, 31, 26
 Barcons, X., et al. 2001, A&A, submitted, preprint (astro-ph/0110269)
 Barger, A. J., Cowie, L. L., Mushotzky, R. F., Richards, E. A. 2001, AJ, 121, 662
 Boyle B.J., Georgantopoulos I., Blair A. J., Stewart G. C., Griffiths R.E., Shanks T., Gunn K.F., Almaini O., 1998, MNRAS, 296, 1
 Ceballos, M.T., Barcons, X. 1996, MNRAS, 282, 493
 Chen L.W., Fabian A.C., Gendrau K.C., 1997, MNRAS, 285, 449
 Colafrancesco S., et al., 2000, A&AS, 144, 187
 Comastri A., Fiore F., Vignali C., Matt G., Perola G.C., La Franca F., 2001, MNRAS, 327, 781
 Comastri A., et al., 2002, in ASP Conf.Ser. 000, Issues in unifications of AGNs, ed. R. Maiolino, A. Marconi and N. Nagar (San Francisco: ASP), in press, preprint (astro-ph/0109117)
 Della Ceca, R., Maccacaro T., Gioia I., Wolter A., Stocke J.T. 1992, ApJ, 389, 491
 Fiore, F., La Franca, F., Giommi, P., Elvis, M., Matt, G., Comastri, A., Molendi, S., Gioia, I. 1999, MNRAS, 306, L55
 Fiore, F. et al. 2000, New Astronomy, 5, 143
 Fiore F., et al., 2001, MNRAS, 327, 771
 Giacconi, R. et al., 2001, ApJ, 551, 624
 Georgantopoulos I., Stewart G.C., Blair A.J., Shanks T., Griffiths R.E., Boyle B.J., Almaini O., Roche N., 1997, MNRAS, 291, 203
 George et al. 2000, ApJ 531, 52
 Gorosobel et al. 1998, A&A, 339, 719
 Grossan, B.A., 1992, PhD Thesis, MIT
 Hasinger, G., et al. 2001, A&A, 365, 45
 Hornschemeier, A. E., et al. 2000, ApJ, 541, 49
 Hornschemeier, A. E., et al. 2001, ApJ, 554, 742
 La Franca, F. & Cristiani, S. 1997, AJ, 113, 1517
 La Franca F., Fiore F., Vignali C., Comastri A., Pompilio F., 2001, in ASP Conf. Ser. 232, The New Era of Wide Field Astronomy, ed. R.G. Clowes, A.J. Adamson & G.E. Bromage (San Francisco: ASP), 96, preprint(astro-ph/00111008)
 Miyaji T., Hasinger G., Schmidt M., 2000, A&A, 353, 25
 Mineo, T. et al. 2000, A&A, 355, 1053
 Mushotzky, R.F., Cowie, L.L., Barger, A.J., Arnaud, K.A. 2000, Nature, 404, 459
 Oke, J. B. 1990, AJ, 99, 1621
 Pompilio F., La Franca F., Matt G., 2000, A&A, 353, 440
 Tozzi, P., et al. 2001, ApJ, 562, 42
 Tresse, L., Rola, C., Hammer, F., Stasinska, G., Le Fevre, O., Lilly, S. J., Crampton, D. 1996, MNRAS, 281, 847
 Ueda, Y. et al. 1998, Nature, 391, 866
 Vecchi, A., Molendi, S., Guainazzi, M., Fiore, F., Parmar, A. N. 1999, A&A, 349, 73
 Vignali, C., Comastri, A., Fiore, F., La Franca, F. 2001, A&A, 370, 900
 Wood, K.S. et al. 1984, ApJS, 56, 507
 Zitelli, V., Mignoli, M., Zamorani, G., Marano, B., Boyle, B. J. 1992, MNRAS, 256, 349

TABLE 1
SKY COVERAGE

Log(Flux) 5-10 keV erg cm ⁻² s ⁻¹	Area deg ²
-10.34	55.51
-11.85	55.51
-11.89	55.48
-11.93	55.39
-11.97	55.28
-12.00	55.05
-12.04	54.66
-12.08	54.04
-12.11	53.16
-12.15	51.97
-12.19	50.63
-12.22	49.04
-12.26	47.13
-12.30	44.88
-12.34	42.44
-12.37	39.93
-12.41	37.49
-12.45	34.88
-12.48	31.93
-12.52	28.83
-12.56	25.67
-12.59	22.75
-12.63	20.03
-12.67	17.53
-12.70	15.23
-12.74	13.16
-12.78	11.32
-12.82	9.73
-12.85	8.30
-12.89	6.96
-12.93	5.67
-12.96	4.56
-13.00	3.60
-13.04	2.88
-13.07	2.35
-13.11	1.96
-13.15	1.60
-13.19	1.27
-13.22	0.94
-13.26	0.68
-13.30	0.47
-13.33	0.33
-13.37	0.22
-13.41	0.14
-13.44	0.08
-13.48	0.05
-13.52	0.03
-13.56	0.01
-13.59	0.00

TABLE 5
EMISSION LINE MEASUREMENTS

Name	z	Type	MgII (Å)	OII (Å)	H β (Å)	OIII (Å)	H α +NII (Å)	SII (Å)
H002636–194416	0.238	FWZI	...	62.1	38.1	62.1
		FWHM	...	19.7	15.4	18.5
		EW	...	82.4	14.6	133.1
H004546–251550	0.111	FWZI	40.1	104.2	44.1
		FWHM	14.6	69.7	50.4
		EW	...	-1.3	-0.2	5.6	22.2	2.5
H012157–584442	0.118	FWZI	...	44.1	38.1	64.1	120.2	48.1
		FWHM	...	19.7	13.1	16.8	45.0	80.0
		EW	...	30.4	2.9	21.4	53.5	20.8
H013434–295816	2.217	FWZI	^a 452.7
		FWHM	^a 123.6
		EW	^a 156.5
H013533–295202	1.344	FWZI	282.5
		FWHM	67.6
		EW	61.2
H033408–360403	0.904	FWZI	412.6	40.1
		FWHM	174.0	26.5
		EW	120.5	6.1
H043712–473148	0.142	FWZI	...	36.0	122.2	64.1	162.3	70.1
		FWHM	...	16.4	36.4	20.9	39.7	73.0
		EW	...	5.2	65.4	23.6	241.2	17.0
H043847–472802	1.453	372.6
		64.9
		61.4
H064638–441534	0.153	FWZI	...	60.1	128.2	60.1	122.2	46.1
		FWHM	...	18.3	47.2	21.3	36.1	29.0
		EW	...	7.9	61.0	78.9	168.4	10.0
H083737+254752	0.077	FWZI	...	52.1	69.4	56.8	327.2	60.1
		FWHM	...	40.3	28.8	15.2	71.8	43.0
		EW	...	51.8	16.0	11.3	291.6	17.0
H083859+260814	0.048	FWZI	36.7	40.1	110.2	70.1
		FWHM	11.7	23.2	42.1	32.2
		EW	...	-8.9	1.9	4.1	46.0	6.7
H103216+505120	0.174	FWZI	...	30.0	203.7	36.7	150.2	33.4
		FWHM	...	12.0	68.1	13.2	79.9	15.0
		EW	...	5.8	65.1	13.1	163.2	6.5
H111814+402838	0.387	FWZI	340.5	50.1	...	40.1
		FWHM	184.0	46.7	...	10.3
		EW	393.8	6.7	-0.7	6.7
H111849+402648	1.129	FWZI	^a 200.3
		FWHM	^a 65.6
		EW	^a 59.9
H121853+295902	0.176	FWZI	...	43.4	36.1	56.8	153.6	50.1
		FWHM	...	12.4	12.1	12.5	26.8	20.9
		EW	...	25.4	17.8	199.6	186.1	22.6
H124028–051402	0.300	FWZI	...	80.1	166.9	63.4
		FWHM	...	25.6	61.3	23.9
		EW	...	36.1	90.8	67.1

NOTE.—Observed frame. Negative values correspond to absorption lines; (a) C IV line.

TABLE 5
EMISSION LINE MEASUREMENTS

Name	z	Type	MgII (Å)	OII (Å)	H β (Å)	OIII (Å)	H α +NII (Å)	SII (Å)
H124036–050752	0.008	FWZI	20.0	-10.0	90.1	76.8
		FWHM	13.9	-7.0	34.0	26.0
		EW	0.8	-0.4	26.3	6.8
H130436–101549	2.386	FWZI	^a 468.7
		FWHM	^a 128.4
		EW	^a 537.0
H134820–301156	0.128	FWZI	...	52.1	...	56.1	112.2	...
		FWHM	...	21.5	...	22.0	53.9	...
		EW	...	19.0	-0.4	12.7	63.0	...
H134845–302946	0.330	FWZI	...	36.0	220.4	72.1
		FWHM	...	15.8	83.0	20.5
		EW	...	2.3	84.2	55.8
H135015–302010	0.074	FWZI	...	60.1	...	52.1	168.3	56.1
		FWHM	...	23.1	...	24.5	64.4	31.7
		EW	...	100.5	-0.6	16.0	48.8	8.0
H135354+182016	0.217	FWZI	...	52.1	24.0	64.1	252.4	40.1
		FWHM	...	13.7	9.3	19.7	95.0	47.9
		EW	...	47.3	2.1	22.8	154.0	12.4
H151934+653558	0.044	FWZI	...	36.0	...	44.1	92.2	44.1
		FWHM	...	13.6	...	9.7	9.0	14.5
		EW	...	43.6	-1.3	22.6	26.4	6.1
H163419+594504	0.341	FWZI	144.2	48.1	72.1	56.1
		FWHM	19.9	12.9	12.9	13.7
		EW	33.1	19.7	30.8	267.2
H165043+043618	0.031	FWZI	...	48.1	36.1	52.1	124.2	56.1
		FWHM	...	40.1	27.2	21.0	49.1	32.6
		EW	...	45.9	2.8	26.6	43.0	12.3
H165238+022206	0.395	FWZI	184.3	56.1	164.3	64.1
		FWHM	70.0	24.1	129.5	21.5
		EW	66.6	22.5	37.5	68.5
H204253–103826	0.363	FWZI	...	72.1	184.3	76.1
		FWHM	...	22.5	48.5	22.3
		EW	...	15.4	73.0	201.8
H204435–102808	2.755	FWZI	^a 248.4
		FWHM	^a 101.9
		EW	^a 56.6
H222632+211138	0.260	FWZI	125.5	26.7
		FWHM	41.6	7.9
		EW	36.4	9.3
H231932–424228	0.101	FWZI	...	68.1	40.1	56.1	172.3	64.1
		FWHM	...	23.1	26.3	21.8	46.9	38.4
		EW	...	20.4	5.0	24.2	77.6	7.5
H232729+084926	0.154	FWZI	...	28.0	92.2	60.1	116.2	56.1
		FWHM	...	15.9	80.3	18.7	34.2	37.5
		EW	...	13.0	16.8	19.1	60.9	16.2
H232906+083416	0.953	FWZI	368.6
		FWHM	76.1
		EW	133.6
H233154+193836	0.475	FWZI	344.5
		FWHM	75.0
		EW	93.5

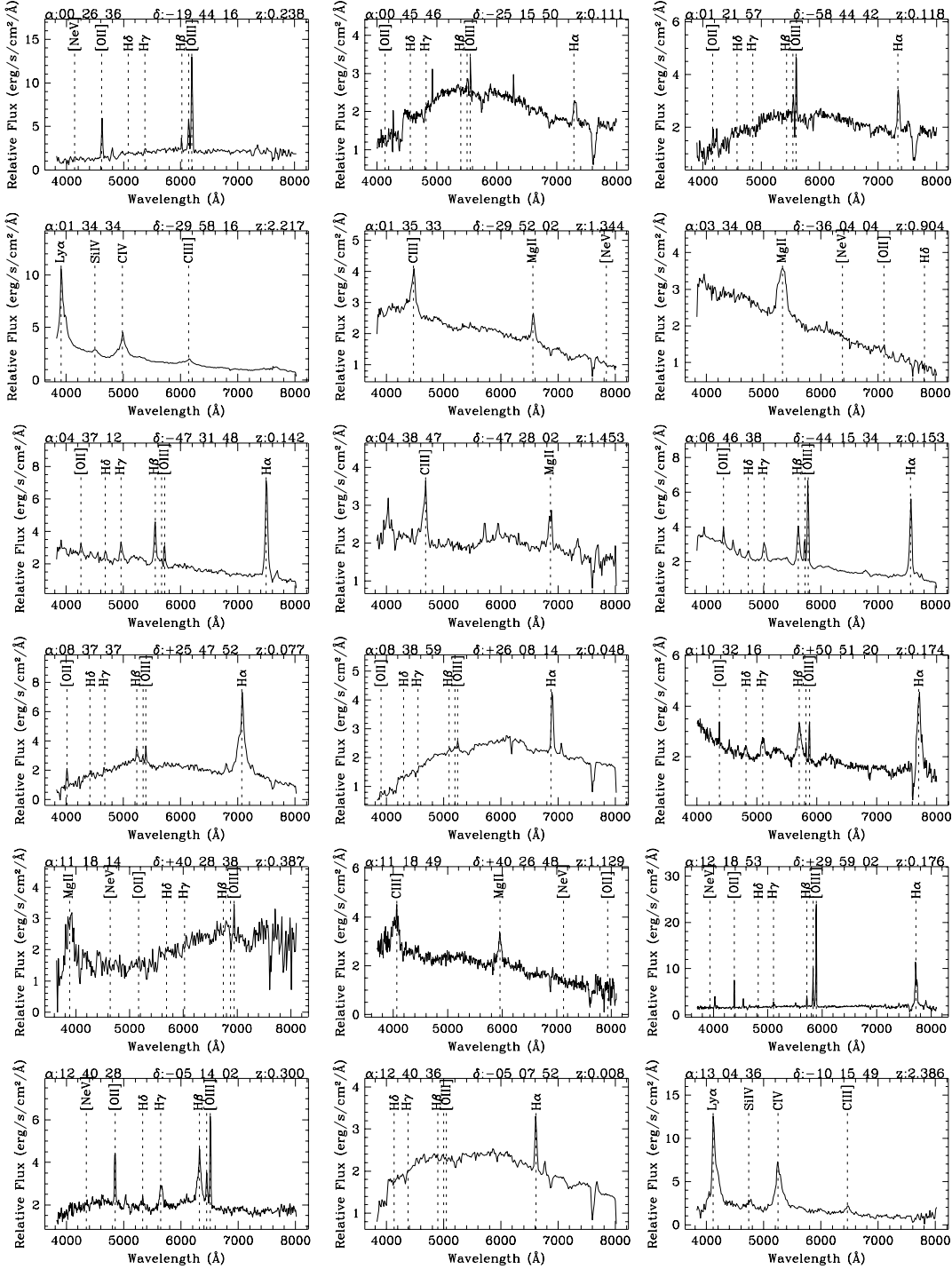


FIG. 3.— The optical spectra of the most probable identified counterparts of the HELLAS sources. The most typical emission lines for AGN are over-plotted with the corresponding redshift.

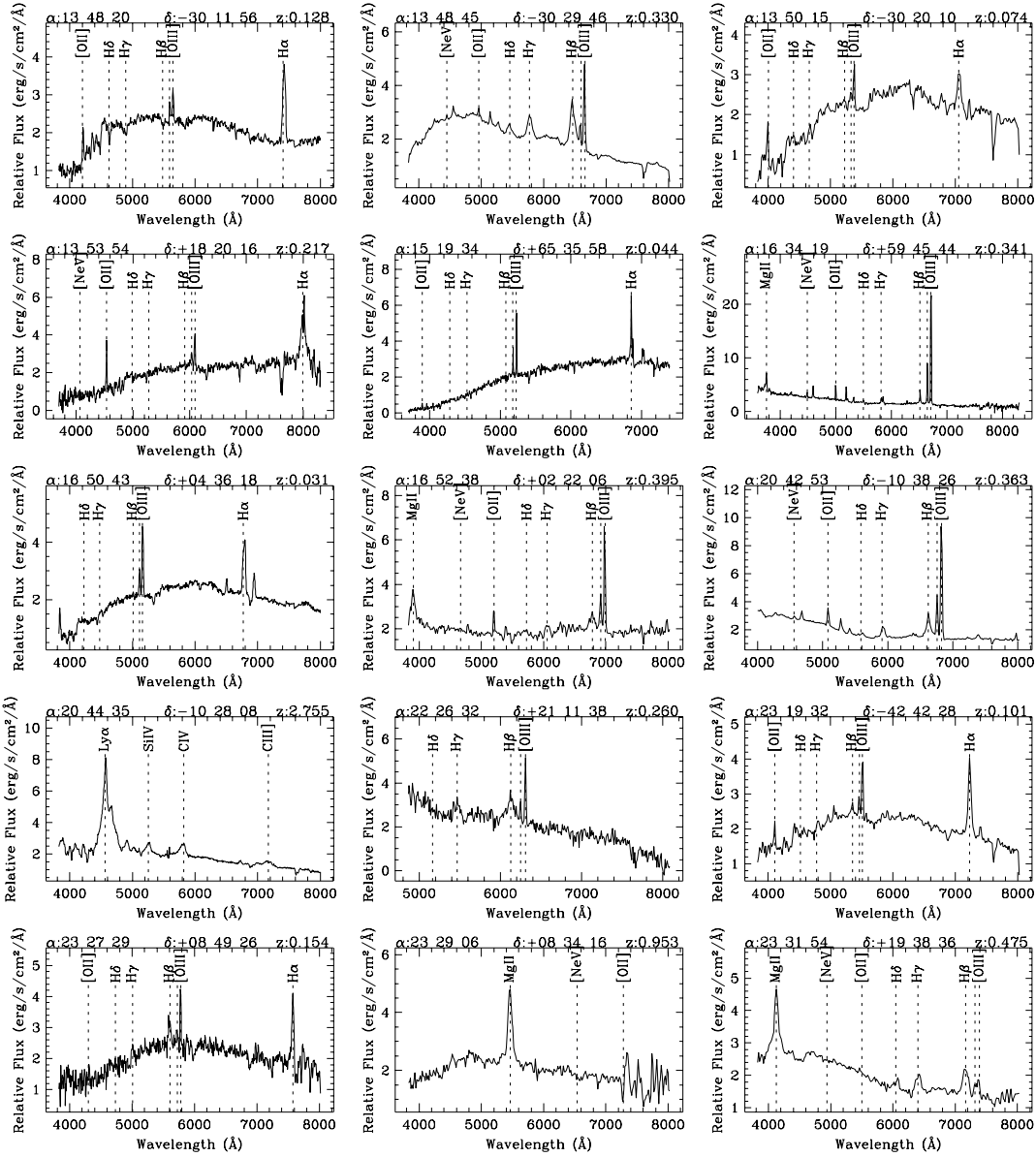


FIG. 3.— continued